

Implications for Ca²⁺-Binding Proteins. Since Cd-O(carboxylate) distances proved to be very similar to Ca-O(carboxylate) distances in the EGTA⁴⁻ complexes and coordination numbers in the two complexes were identical, one infers that the Cd²⁺ ion is a good choice as a spectroscopic probe for calcium-binding site structure. However, it should be noted that calcium-selective proteins utilize neutral oxygen donors (carbonyl oxygen atoms and hydroxyl groups) as well as anionic carboxylate donors to bind Ca²⁺. Substitution of Cd²⁺ for Ca²⁺ at a protein metal-binding site results, as noted above, in observation of a highly shielded ¹¹³Cd resonance. Since the Cd²⁺ ion has shown a distinctly lower affinity for neutral oxygen donors than Ca²⁺ in the present study, and since long Cd-O distances are thought to be associated with highly shielded chemical shift values from single-crystal NMR studies, the low affinity of Cd²⁺ for neutral oxygen donors, rather than intrinsic site structure, may be responsible for the highly shielded chemical shift values characteristic of the cadmium-substituted proteins.

Acknowledgment. The Nicolet R3m/E X-ray diffractometer and computing system at Colorado State University was purchased

with funds provided by the National Science Foundation. Solid-state ¹¹³Cd NMR spectra were recorded in the Colorado State University Regional NMR Center, funded by the National Science Foundation. We thank Dr. Bruce Hawkins for obtaining the ¹¹³Cd solid-state NMR spectra.

Supplementary Material Available: Table S-I—chelate ring conformational parameters for **1**, Table S-II—inter-ring torsion angles for **1**, Table S-III—anisotropic thermal parameters for **1**, Table S-IV—calculated hydrogen atom coordinates for **1**, Table S-VI—chelate ring conformational parameters for **2**, Table S-VII—inter-ring torsion angles for **2**, Table S-VIII—anisotropic thermal parameters for **2**, Table S-IX—calculated hydrogen atom coordinates for **2**, Table S-XI—selected least-squares planes for **1**, Table S-XII—hydrogen bonding distances in **1**, Table S-XIII—selected least-squares planes for **2**, Table S-XIV—hydrogen bonding distances in **2**, Figure S-1—view of the unit cell of **1**, and Figure S-2—view of the unit cell of **2** (26 pages); Tables S-V and S-X—observed and calculated structure factors, ×10, for **1** and **2**, respectively (86 pages). Ordering information is given on any current masthead page.

Crystal and Molecular Structure of the Charge-Transfer Salt of Decamethylcobaltocene and Tetracyanoethylene (2:1): $\{[\text{Co}(\text{C}_5\text{Me}_5)_2]^+\}_2[\text{C}(\text{CN})_2\text{CC}(\text{CN})_2]^{2-}$. The Electronic Structures and Spectra of $[\text{TCNE}]^n$ ($n = 0, 1-, 2-$)

David A. Dixon* and Joel S. Miller*

Contribution No. 4175 from the Central Research and Development Department, E. I. du Pont de Nemours & Co., Experimental Station E328, Wilmington, Delaware 19898. Received August 15, 1986

Abstract: The reaction of decamethylcobaltocene, $\text{Co}(\text{C}_5\text{Me}_5)_2$, and tetracyanoethylene, TCNE, leads to the isolation of two phases of 1:1 and 2:1 composition. The crystal and molecular structure of the 2:1 substance has been determined by single-crystal X-ray analysis at -50°C . The red-orange 2:1 complex crystallizes as the acetonitrile solvate in the triclinic $P1$ space group (No. 2) [$a = 10.579$ (6) Å, $b = 14.142$ (7) Å, $c = 15.939$ (5) Å, $\alpha = 114.73$ (3)°, $\beta = 94.40$ (4)°, $\gamma = 91.48$ (4)°, $V = 2155$ (4) Å³, and $Z = 2$]. The unit cell is comprised of two independent $[\text{Co}(\text{C}_5\text{Me}_5)_2]^+$ cations, an anion, and a MeCN solvent molecule. The final weighted R_w was 0.083. The $\text{C}_5\text{Co}^{\text{III}}$ cation is ordered and is essentially structurally equivalent to the isoelectronic $\text{Fe}^{\text{I}}(\text{C}_5\text{Me}_5)_2$; however, the average C-C and $\text{Co}^{\text{III}}-\text{C}_5$ ring distances are ~ 0.04 Å shorter than the analogous distances observed for $[\text{Fe}^{\text{III}}(\text{C}_5\text{Me}_5)_2]^+$. The dianion structure possesses approximate D_{2d} local symmetry with C-C and average C-CN and C≡N distances of 1.49 (2), 1.392 (8), and 1.166 (3) Å, respectively. The $[\text{C}(\text{CN})_2]^-$ groups have an $87.1 \pm 0.3^\circ$ dihedral angle. For the $[\text{TCNE}]^n$ series for $n = 0$ the C-CN distance is greater than the C-C distance; for $n = 2-$ the converse is true, and for $n = 1-$ the distances are comparable. The $[\text{TCNE}]^n$ ($n = 0, 1-, 2-$) moieties have been characterized by infrared, Raman, and UV-vis spectroscopic techniques. The electronic absorption spectra of $[\text{TCNE}]^n$ exhibits a band ($\lambda_{\text{max}} \approx 23375 \text{ cm}^{-1}$; $\epsilon \sim 8425 \text{ M}^{-1} \text{ cm}^{-1}$) with a progression of 17 vibrational transitions ($\sim 550 \text{ cm}^{-1}$) tentatively assigned to coupling of the excited-state C-CN bend to the $\Pi-\Pi^*$ transition. TCNE exhibits a $\Pi \rightarrow \Pi^*$ transition at 38300 cm^{-1} with four vibrational overtones ($\sim 1200 \text{ cm}^{-1}$) tentatively assigned to coupling to the $\nu(\text{C}=\text{C})$ vibration. The electronic structures of $[\text{TCNE}]^n$ ($n = 0, 1-, 2-$) have been calculated by ab initio molecular orbital theory with the STO-3G basis set and additionally for $n = 0$ and $2-$ with a double- ζ basis set augmented by a set of d polarization functions at the ethylene sp^2 carbons. The latter method gives results that are in good agreement with those obtained with ab initio STO-3G basis sets. The geometries were determined with both basis sets. The force fields were determined with both basis sets, and the frequencies are compared to the experimental values. These results confirm the D_{2h} and D_{2d} structures of $[\text{TCNE}]^-$ and $[\text{TCNE}]^{2-}$, respectively. Charge and spin distributions are presented and are discussed in terms of classical resonance structures.

Since our observation of molecular metamagnetism^{1,2} and ferromagnetism^{2,3} for the 1:1 TCNQ and TCNE (TCNQ = 7,7,8,8-tetracyano-*p*-quinodimethane; TCNE = tetracyanoethylene) salts of decamethylferrocene, respectively, we have sought to understand the structure-function relationship of me-

talocenium salts of strong acceptor anions with the particular focus on understanding the microscopic basis for cooperative magnetic phenomena in molecular materials. With our recent discovery of the means to stabilize dianionic acceptors⁴ enabling their structural and spectroscopic characterization, we have prepared $\{[\text{Co}(\text{C}_5\text{Me}_5)_2]^+\}_2[\text{TCNE}]^{2-}$ and studied its physical properties. We are particularly interested in this compound as it allows comparison with other percyano anions and also provides a closed-shell model compound with which to compare other cyano

(1) Candela, G. A.; Swartzendruber, L. J.; Miller, J. S.; Rice, M. J. *J. Am. Chem. Soc.* **1979**, *101*, 2755.

(2) Miller, J. S.; Epstein, A. J.; Reiff, W. M. *Isr. J. Chem.*, in press.

(3) (a) Miller, J. S.; Calabrese, J. C.; Epstein, A. J.; Bigelow, R. W.; Zhang, J. H.; Reiff, W. M. *J. Chem. Soc., Chem. Commun.* **1986**, 1026. (b) Miller, J. S.; Calabrese, J. C.; Chittapeddi, S. R.; Zhang, J. H.; Reiff, W. H.; Epstein, A. J. *J. Am. Chem. Soc.* **1987**, *109*, 769.

(4) Miller, J. S.; Dixon, D. A. *Science (Washington, D.C.)* **1987**, *235*, 871.

radical anion complexes and complements our previous work on $[C(CN)_3]^-$.⁵

Experimental Section

$\{[Co(C_5Me_5)_2]^+[(NC)_2CC(CN)_2]^{2-}\} \cdot MeCN$ was prepared from $Co(C_5Me_5)_2$ and TCNE in an inert atmosphere glovebox. Decamethylcobaltocene (120 mg, 0.364 mmol; Strem), prepared from decamethylcobaltocenium hexafluorophosphate,⁶ was dissolved in 30 mL of hot acetonitrile (distilled under argon from P_2O_5 and subsequently CaH_2). This solution was added to 23 mg (0.182 mmol) of TCNE dissolved in 2 mL of MeCN. After the volume was reduced by one-half via distillation of the solvent, the solution was refrigerated at $-25^\circ C$ overnight; 110 mg of the red-orange product (73%) was collected by vacuum filtration. Elemental Anal. (Galbraith, Knoxville, TN) for $C_{48}H_{63}Co_2N_5$: Calcd: C, 69.64; H, 7.67; Co, 14.24; N, 8.46. Found: C, 69.72; H, 7.88; N, 8.74. Infrared spectra (Nujol): $\nu(C\equiv N)$ 2069 s and 2140 s cm^{-1} . The $[M-(C_5Me_5)_2]^+[(TCNE)]^{2-}$ ($M = Fe, Co$) salts were prepared as previously reported.^{3b}

X-ray Data Collection and Data Reduction. A red-orange irregularly shaped crystal having approximate dimensions of $0.13 \times 0.27 \times 0.47$ mm was mounted in a glass capillary with its long axis roughly parallel to the ϕ axis of the goniometer. Preliminary examination and data collection were performed with Mo $K\alpha$ radiation ($\lambda = 0.71073 \text{ \AA}$) on an Enraf-Nonius CAD4 computer-controlled κ axis diffractometer equipped with a graphite crystal, incident beam monochromator.⁷

Cell constants and an orientation matrix for data collection were obtained from least-squares refinement, using the setting angles of 18 reflections in the range $7^\circ < \theta < 14^\circ$, measured by the computer-controlled diagonal slit method of centering. The triclinic cell parameters and calculated volume are $a = 10.579(6) \text{ \AA}$, $b = 14.142(7) \text{ \AA}$, $c = 15.939(5) \text{ \AA}$, $\alpha = 114.73(3)^\circ$, $\beta = 94.40(4)^\circ$, $\gamma = 91.48(4)^\circ$, and $V = 2155(4) \text{ \AA}^3$. For $Z = 2$ and $M_r = 827.94$ daltons the calculated density is 1.28 g/cm^3 . As a check on crystal quality, ω scans of several intense reflections were measured; the width at half-height was 0.22° with a takeoff angle of 2.8° , indicating good crystal quality. There were no systematic absences, and the space group was determined to be $P1$ (No. 2).

The data were collected $-50(1)^\circ C$ by using the ω - θ scan technique. The scan rate varied from 2 to $5^\circ/\text{min}$ (in ω). Data were collected to a maximum 2θ of 44.0° . The scan range (in deg) was determined as a function of θ to correct for the separation of the $K\alpha$ doublet; the scan width was calculated as $\theta_{\text{scanwidth}} = (1.0 + 0.140 \tan \theta)^\circ$. Moving-crystal, moving-counter background counts were made by scanning an additional 25% above and below this range, giving a ratio of peak counting time to background counting time of 2:1. The horizontal counter aperture was also adjusted as a function of θ (ranging from 2.0 to 2.4 mm); the vertical aperture was set at 4.0 mm. The diameter of the incident beam collimator was 0.7 mm, and the crystal-to-detector distance was 21 cm. For intense reflections an attenuator (factor = 19.4) was automatically inserted in front of the detector.

Of a total of 5280 reflections collected, 5163 were unique. As a check on crystal and electronic stability, three representative reflections were measured every 30 min. The slope of the least-squares line through a plot of intensity, I , vs. time was 13(2) counts/h which corresponds to a total gain in intensity of 9.0%. An anisotropic decay correction was applied. The correction factors on I ranged from 0.973 to 1.283 with an average value of 1.022. Lorentz and polarization corrections were applied to the data. The linear absorption coefficient is 8.0 cm^{-1} for Mo $K\alpha$ radiation. No absorption correction was made.

Structure Solution and Refinement. The structure was solved by direct methods. With use of 449 reflections (minimum E of 1.65) and 5548 relationships, a total of 32 phase sets were produced. A total of two atoms were located from an E map prepared from the phase set with probability statistics: absolute figure of merit = 1.17, residual = 8.23, and $\psi_0 = 2715$. The remaining atoms were located in succeeding difference Fourier syntheses. Hydrogen atoms were not included in the calculations. The structure was refined in full-matrix least squares where the function minimized was $\sum w(|F_o| - |F_c|)^2$ and the weight w is defined as $4F_o^2/\sigma^2(F_o^2)$.

The standard deviation on intensities, $\sigma(F_o^2)$, is defined in eq 1, where

$$\sigma^2(F_o^2) = [S^2(C + R^2B) + (pF_o^2)^2]/L_p^2 \quad (1)$$

S is the scan rate, C is the total integrated peak count, R is the ratio of

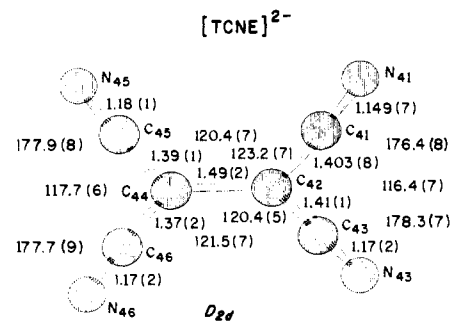


Figure 1. Atom labeling and bond distances and angles for $[TCNE]^{2-}$.

scan time to background counting time, B is the total background count, L_p is the Lorentz-polarization factor, and the parameter p (set to 0.060) is a factor introduced to downweight intense reflections.

Neutral atom scattering factors were taken from Cromer and Waber.^{8a} Anomalous dispersion effects were included in F_o ;^{8a} the values for f' and f'' were those of Cromer.^{8b} Only the 3751 reflections having intensities greater than 3.0 times their standard deviation were used in the refinements. The final cycle of refinement included 496 variable parameters and converged (largest parameter shift was 0.05 times its estimated standard deviation) with unweighted, R , and weighted, R_w , agreement factors of

$$R = \sum ||F_o| - |F_c|| / \sum |F_o| = 0.069$$

$$R_w = (\sum w(|F_o| - |F_c|)^2 / \sum wF_o^2)^{1/2} = 0.083$$

The standard deviation of an observation of unit weight was 2.55. There were 88 correlation coefficients greater than 0.50. The highest correlation coefficient was 0.70 between parameters 394 and 397. The highest peak in the final difference Fourier had a height of 0.59 $e/\text{\AA}^3$ with an estimated error based on ΔF^{9b} of 0.11. As hydrogens were not refined, this peak is assigned to a methyl hydrogen 0.9 \AA from C16. Plots of $\sum w(|F_o| - |F_c|)$ vs. $|F_o|$, reflection order in data collection, $(\sin \theta)/\lambda$, and various classes of indices showed no unusual trends. All calculations were performed on a VAX-11/750 computer using SDP-PLUS.¹⁰

Spectroscopic Measurements. The infrared and Raman spectra were recorded on a Nicolet 7199 Fourier transform and J-Y Raman microprobe spectrometers, respectively. The UV-visible spectra were recorded on a Cary 2390 or a Spex 222 spectrometer.

Molecular Orbital Calculations. The geometries for $[C_2(CN)_4]^n$ ($n = 0, 1, -2$) were gradient optimized¹¹ at the SCF level with the HONDO program¹² on an IBM 3081 computer. For the closed shell species with $n = 0$ and $n = -2$, the geometries were optimized in the RHF framework with both the STO-3G¹³ and a double- ζ basis set augmented by a set of d polarization functions ($\zeta(3d) = 0.75$)¹⁴ on the ethylene sp^2 carbons ($DZ + D_C$). The double- ζ portion of the basis set has the form (9,5)/[3,2] with all exponents and coefficients from Dunning and Hay.¹⁴ The $DZ + D_C$ basis set has been used in an extensive study of fluorocarbons¹⁵ and has previously been shown to give reliable geometric and energetic predictions. In order to examine the role of diffuse functions, we augmented the $DZ + D_C$ basis set with a set of s and p diffuse functions on the

(8) (a) Cromer, D. T.; Waber, J. T. *International Tables for X-Ray Crystallography*; The Kynoch Press: Birmingham, England, 1974; Vol. IV, Table 2.2B. (b) Cromer, D. T. *International Tables for X-Ray Crystallography*; The Kynoch Press: Birmingham, England, 1974; Vol. IV, Table 2.3.1.

(9) (a) Ibers, J. A.; Hamilton, W. C. *Acta Crystallogr.* **1964**, *17*, 781. (b) Cruickshank, D. W. J. *Acta Crystallogr.* **1949**, *2*, 154.

(10) Frenz, B. A. In *Computing in Crystallography*; Schenk, H., Olthoff-Hazelkamp, R.; van Koningsveld, H.; Bassi, G. C., Eds. Delft University Press: Delft, Holland, 1978; p 64.

(11) (a) Komornicki, A.; Ishida, K.; Morokuma, K.; Ditchfield, R.; Conrad, M. *Chem. Phys. Lett.* **1977**, *45*, 595. McIver, J. A.; Komornicki, A. Jr. *Ibid.* **1971**, *10*, 303. (b) Pulay, P. In *Applications of Electronic Structure Theory*; Schaefer, H. F., III, Ed.; Plenum: New York, 1977; p 153.

(12) (a) Dupuis, M.; Rys, J.; King, H. F. *J. Chem. Phys.* **1976**, *65*, 111. (b) King, H. F.; Dupuis, M.; Rys, J. *National Resource for Computer Chemistry Software Catalog, Vol. 1*, Program QHO2 (HONDO), 1980.

(13) Hehre, W. J.; Stewart, R. F.; Pople, J. A. *J. Chem. Phys.* **1969**, *51*, 2657.

(14) Dunning, T. H., Jr.; Hay, P. J. In *Methods of Electronic Structure Theory*; Schaefer, H. F., III, Ed.; Plenum: New York, 1977; Chapter 1.

(15) (a) Dixon, D. A.; Fukunaga, T.; Smart, B. E. *J. Am. Chem. Soc.* **1986**, *108*, 1585. (b) Dixon, D. A.; Fukunaga, T.; Smart, B. E. *J. Am. Chem. Soc.* **1986**, *108*, 4027.

(5) Dixon, D. A.; Calabrese, J. C.; Miller, J. S. *J. Am. Chem. Soc.* **1986**, *108*, 2582.

(6) Robbins, J. L.; Edelstein, M.; Spenser, B.; Smart, J. C. *J. Am. Chem. Soc.* **1982**, *104*, 1882.

(7) Onieda Research Services, Inc., Whitesboro, NY 13492.

Table I. Intramolecular Bond Distances (Å) for $[\text{Co}(\text{C}_5\text{Me}_5)_2]_2[\text{TCNE}]\cdot\text{MeCN}^a$

atom 1	atom 2	dist	atom 1	atom 2	dist	atom 1	atom 2	dist
Co1	C1	2.036 (7)	N50	C51	1.14 (2)	C22	C23	1.420 (9)
Co1	C2	2.077 (7)	C1	C2	1.43 (1)	C22	C27	1.49 (1)
Co1	C3	2.040 (7)	C1	C5	1.40 (2)	C23	C24	1.40 (1)
Co1	C4	2.052 (5)	C1	C6	1.52 (1)	C23	C28	1.531 (8)
Co1	C5	2.048 (6)	C2	C3	1.43 (1)	C24	C25	1.403 (8)
Co1	C11	2.021 (6)	C2	C7	1.52 (2)	C24	C29	1.542 (9)
Co1	C12	2.071 (6)	C3	C4	1.41 (1)	C25	C30	1.51 (2)
Co1	C13	2.065 (6)	C3	C8	1.53 (1)	C31	C32	1.41 (1)
Co1	C14	2.041 (7)	C4	C5	1.46 (2)	C31	C35	1.379 (9)
Co1	C15	2.051 (7)	C4	C9	1.48 (1)	C31	C36	1.516 (8)
Co2	C21	2.047 (6)	C5	C10	1.52 (1)	C32	C33	1.425 (8)
Co2	C22	2.054 (8)	C11	C12	1.46 (2)	C32	C37	1.54 (1)
Co2	C23	2.030 (8)	C11	C15	1.40 (2)	C33	C34	1.44 (1)
Co2	C24	2.036 (8)	C11	C16	1.51 (1)	C33	C38	1.53 (1)
Co2	C25	2.036 (8)	C12	C13	1.46 (1)	C34	C35	1.424 (8)
Co2	C31	2.041 (7)	C12	C17	1.47 (1)	C34	C39	1.50 (2)
Co2	C32	2.024 (8)	C13	C14	1.43 (1)	C35	C40	1.51 (2)
Co2	C33	2.037 (7)	C13	C18	1.49 (2)	C41	C42	1.403 (8)
Co2	C34	2.066 (7)	C14	C15	1.40 (1)	C42	C43	1.41 (1)
Co2	C35	2.052 (7)	C14	C19	1.53 (1)	C42	C44	1.49 (2)
N41	C41	1.149 (7)	C15	C20	1.56 (2)	C44	C45	1.39 (1)
N43	C43	1.17 (2)	C21	C22	1.44 (1)	C44	C46	1.37 (2)
N45	C45	1.18 (1)	C21	C25	1.43 (2)	C51	C52	1.39 (2)
N46	C46	1.17 (1)	C21	C26	1.518 (9)			

^a Numbers in parentheses are estimated standard deviations in the least significant digits.

Table II. Summary of Bond Distances for $[\text{M}(\text{C}_5\text{Me}_5)_2]^n$ (M = Co, Fe)^a

	<i>n</i>	M-C	C-C	C-Me	M-C ₅ ^b	ref
Fe ^{II}	0	2.050	1.419	1.502	1.656	3b
Fe ^{III}	1+	2.092	1.418	1.503	1.703	3b
Co ^{III}	1+	2.051	1.422	1.52	1.651	this work

^aIn Å. ^bRing centroid.

ethyleneic carbons (DZ + D_C + Dif) and subsequently added a set of s and p diffuse functions to all atoms (DZ + D_C + All). The exponent for the diffuse p function was taken from Dunning and Hay,¹⁴ whereas the exponent for the diffuse s function was obtained by geometric extrapolation using the ratio found for the diffuse p function. The geometries for the dianion were gradient-optimized with these two basis sets. The force fields with the STO-3G and DZ + D_C basis sets for the closed-shell species were obtained analytically¹⁶ with the program GRADSCF¹⁷ on a CRAY/1A computer. The force field for the dianion was also calculated with the DZ + D_C + Dif basis set. The geometry of the open-shell doublet anion was obtained in the UHF framework by gradient techniques only at the STO-3G level. The force field for *n* = 1- was obtained by numerical differentiation of the gradient with the program HONDO.

Results and Discussion

Crystal Structure. $[\text{Co}(\text{C}_5\text{Me}_5)_2]_2[\text{TCNE}]\cdot\text{MeCN}$. The triclinic unit cell is comprised of two independent ordered cations, an independent anion and a solvent molecule. The bond distances are given in Table I. The fractional coordinates, anisotropic thermal parameters, general temperature factors, and interatomic angles as well as weighted least square planes are given as supplementary material. Atom labeling for the anion and pair of independent cations can be found in Figures 1 and 2, respectively.

$[\text{Co}(\text{C}_5\text{Me}_5)_2]^+$. The cations, Figure 2, are ordered with C₅ local symmetry possessing distances essentially equivalent to the iso-electronic Fe^{II}(C₅Me₅)₂ (Table II). The Co^{III}-C, C-C, and C-Me separations range between 2.021 (6) and 2.077 (7) Å, 1.379 (9) and 1.46 (2) Å, and 1.47 (1) and 1.542 (9) Å and average 2.051, 1.422, and 1.52 Å, respectively. The Co^{III}-C₅ ring centroid ranges from 1.646 to 1.653 Å with an average of 1.651 Å. The Co^{III}-C distance is 0.04 Å shorter than that of $[\text{Fe}^{\text{II}}(\text{C}_5\text{Me}_5)_2]^{2+}$ but

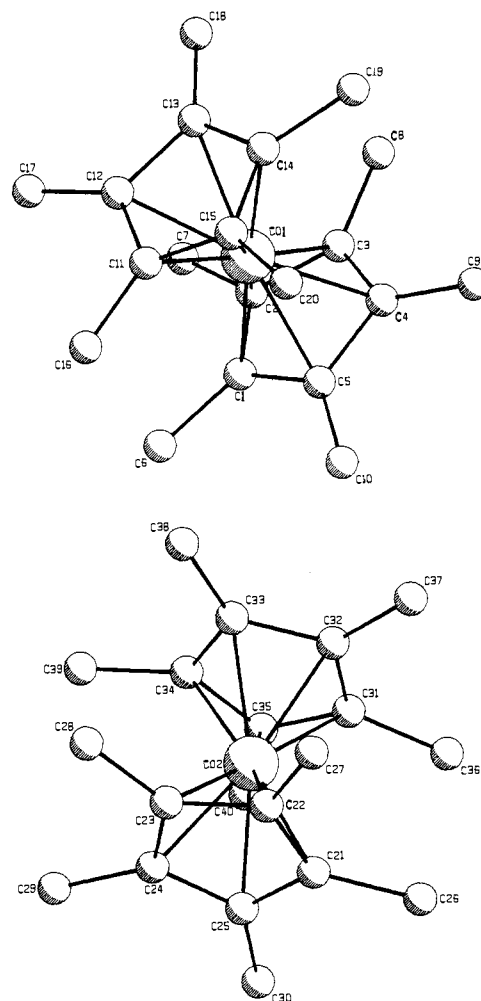


Figure 2. Atom labeling for each independent $[\text{Co}(\text{C}_5\text{Me}_5)_2]^+$.

identical to the Fe^{II} analogue. Likewise the Co^{III}-C₅ ring centroid of 1.651 Å is essentially identical with that of Fe^{II}(C₅Me₅)₂ (1.651 Å) and ~0.05 Å shorter than that of $[\text{Fe}^{\text{III}}(\text{C}_5\text{Me}_5)_2]^{2+}$.^{3b}

$[\text{TCNE}]^{2-}$. The structure of the dianion has been determined for the first time and is of interest particularly for comparison to the structures of TCNE¹⁸ and $[\text{TCNE}]^{\cdot-}$. We recently reported

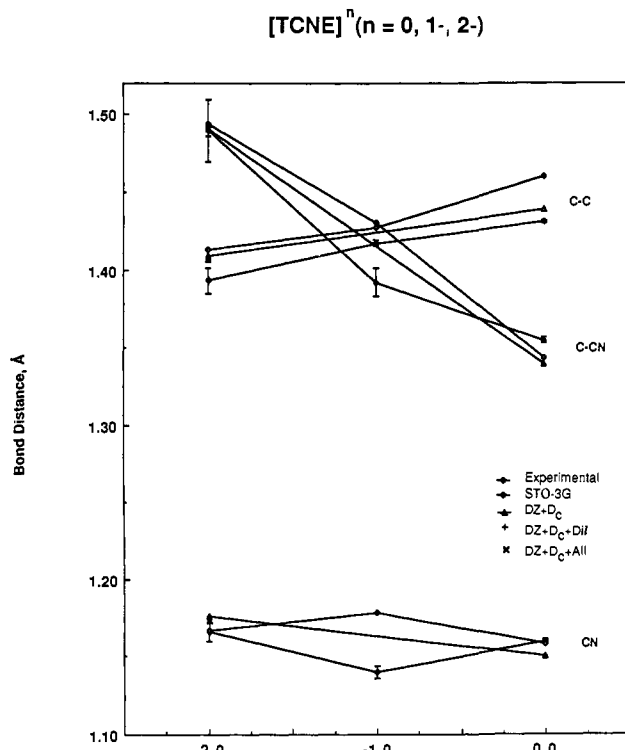
(16) King, H. F.; Komornicki, A. In *Geometrical Derivatives of Energy Surfaces and Molecular Properties*; Jorgenson, P.; Simon, S. J., Eds.; Reidel, D.: Dordrecht, 1986; NATO ASI series C. Vol. 166, p 207. King, H. F.; Komornicki, A. *J. Chem. Phys.* **1986**, *84*, 5645.

(17) GRADSCF is an ab initio gradient program system designed and written by A. Komornicki at Polyatomics Research and supported on grants through NASA-Ames Research Center.

Table III. Crystallographically Determined Bond Lengths and Angles for $[TCNE]^n$ ($n = 0, 1-, 2-$)

diffractn technique	TCNE				[TCNE] ^{••a}	[TCNE] ₂ ^{2-b}	[TCNE] ²⁻
	X-ray	X-ray double atom	neutron	electron	X-ray	X-ray	X-ray
symmetry	D_{2h}	D_{2h}	D_{2h}	D_{2h}	D_{2h}	D_{2h}	D_{2d}
temp, °C					-30	-120	-50
C—C, Å	1.344 (4)	1.358 (3)	1.355 (2)		1.392 (9)	1.35 (2)	1.49 (2)
C—CN, Å	1.439 (2)	1.431 (2)	1.432 (1)	1.435	1.417 (2)	1.46	1.392 (8)
C≡N, Å	1.153 (2)	1.166 (2)	1.160 (1)	1.162	1.140 (4)	1.13	1.166 (3)
C—C≡N, deg			177.93 (7)		179.9	175.0	177.6
NC—C—CN, deg			116.11 (8)		117.7	118.5	117.1
deviatn out of plane, deg	0	0	0	0	0	15	d
R_w %			3.4		5.4	13.1	8.3
ref	18	18	18	18	2b	19	this work
dimer separatr, Å	3.05, 3.50	...

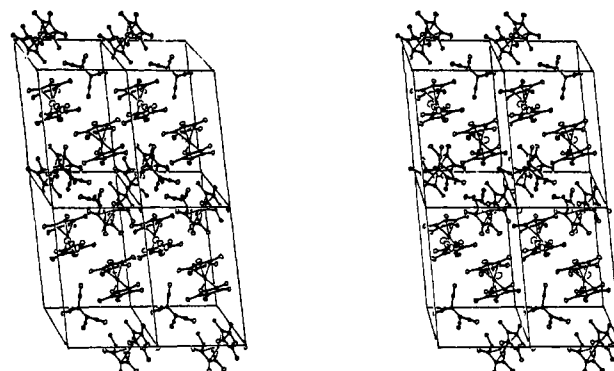
^a Cation: $[Fe(C_5Me_5)_2]^{2+}$. ^b Cation: $[Fe(C_5H_4)_2C_3H_6]^{2+}$. ^c b_{3g} out-of-plane vibration distortion. ^d The dihedral angle between $(NC)_2C$ groups is 87.1° .

**Figure 3.** Bond distances of $[TCNE]^n$ as a function of n .

the structure of the isolated monoanion.^{3b} The details of the structure for $[TCNE]^{2-}$ are given in Figure 1, and Table III summarizes the $[TCNE]^n$ ($n = 0, 1-, 2-$) structural data. This dianion, unlike both TCNE and $[TCNE]^{•-}$ which have planar D_{2h} symmetry, possesses local crystallographic D_{2d} symmetry. The two $[C(CN)_2]^-$ groups are essentially perpendicular to each other and have an $87.1 \pm 0.3^\circ$ dihedral angle (see Figure 1). The central formal C—C single bond is 1.49 (2) Å which is 0.1 and ~ 0.15 Å longer than the C=C bonds for $[TCNE]^n$ ($n = 1-$ and 0), respectively. The C—CN bond distance in $[TCNE]^{2-}$ varies from 1.37 (2) to 1.41 (1) Å and averages 1.392 (8) Å. This is shorter than the average observed for $[TCNE]^{•-}$ and TCNE by 0.05 (3) Å, respectively. The C≡N bond distance ranges from 1.149 (7) to 1.18 (1) Å and averages 1.166 (6) Å which is longer than that reported for TCNE and $[TCNE]^{•-}$ by ~ 0.01 and 0.03 Å, respectively. The NC—C—CN angle ranges from 116.4 (7) to 117.7 (6)°, averaging 117.1°, and is comparable to the values observed for $[TCNE]^n$ ($n = 0$ and 1-). The bond distances as a function of n for $[TCNE]^n$ are summarized in Figure 3.

(18) Becker, P.; Coppens, P.; Ross, R. K. *J. Am. Chem. Soc.* **1973**, *95*, 7604.

(19) Lemervoskii, D. A.; Stukan, R. A.; Tarasevich, B. N.; Slovokhotov, Yu. L.; Antipin, M. Yu.; Kalinin, A. E.; Struchov, Yu. T. *Struct. Khim.* **1981**, *7*, 240.

**Figure 4.** Stereoview of four unit cells of $[Co(C_5Me_5)_2]_2[TCNE] \cdot MeCN$.

The observed bond distances are in good agreement with those obtained from molecular orbital calculations (vide infra). The experimental values show the following variations with charge. The central C—C bond distance increases with increasing negative charge with an increase of ~ 0.04 Å from $n = 0$ to $n = 1-$ and an increase of ~ 0.10 Å from $n = 1-$ to $n = 2-$. The C—CN bond distance first increases from $n = 0$ to $n = 1-$ and then decreases so that $r(C-CN)$ for $n = 2-$ is less than that for $n = 0$. Thus, for $n = 0$ the C—CN distance is greater than the C—C distance; the converse is true for $n = 2-$, and the values are comparable for $n = 1-$. This is also seen for $[TCNQ]^{•-}$ ^{20a} and $[TCNQF_4]^{•-}$.^{20b,c} The C≡N bond distance decreases from $n = 0$ to $n = 1-$ and then increases for $n = 2-$. The significance and accuracy of this trend is hard to determine because of the difficulty in determining $r(C\equiv N)$ in X-ray diffraction experiments.⁵ The NC—C—CN bond angle is observed to increase and then decrease as the amount of negative charge increases. The magnitude is small and not considered significant.

Solid-State Structure. The solid is comprised of segregated columns of cations and anions and is best seen in the stereoview (Figure 4). The cations in their columns are canted with respect to each other, and there are no significant interatomic separations less than the sum of the van der Waals radii.

Spectroscopic Properties

Vibrational Spectra. The Raman spectrum for TCNE shows two cyano stretching bands at 2230 and 2242 cm^{-1} and a C=C stretch at 1570 cm^{-1} . The vibrational spectrum for TCNE has previously been studied in detail.²¹ The C≡N stretches are predicted to be at 2235 (a_g), 2260^{21a} or 2230^{21bc} (b_{1u}), 2247 (b_{2g}),

(20) (a) Miller, J. S.; Zhang, J. H.; Reiff, W. M.; Dixon, D. A.; Preston, L. D.; Reis, A. H., Jr.; Gebert, E.; Extene, M.; Troup, J.; Epstein, A. J.; Ward, M. D. *J. Phys. Chem.*, in press. (b) Miller, J. S.; Zhang, J. H.; Reiff, W. M., submitted for publication. (c) Dixon, D. A.; Miller, J. S., manuscript in preparation.

(21) (a) Miller, F. A.; Sala, O.; Devlin, P.; Overend, J.; Lippert, E.; Lunder, W.; Moser, J.; Varchim, J. *Spectrochim Acta* **1964**, *20*, 1233. (b) Hinkel, J. J.; Devlin, J. P. *J. Chem. Phys.* **1973**, *58*, 4750. (c) Stanley, J.; Smith, D.; Latimer, B.; Devlin, J. P. *J. Phys. Chem.* **1966**, *70*, 2011.

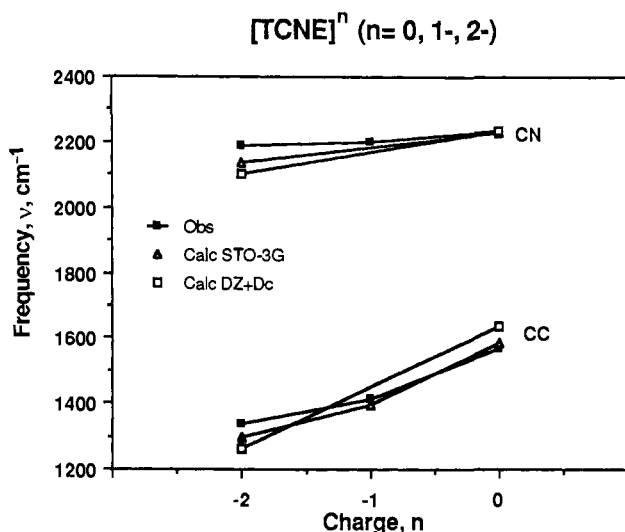


Figure 5. Vibrational frequencies ($\text{C}\equiv\text{N}$ and $\text{C}=\text{C}$) for $[\text{TCNQ}]^n$ as a function of n .

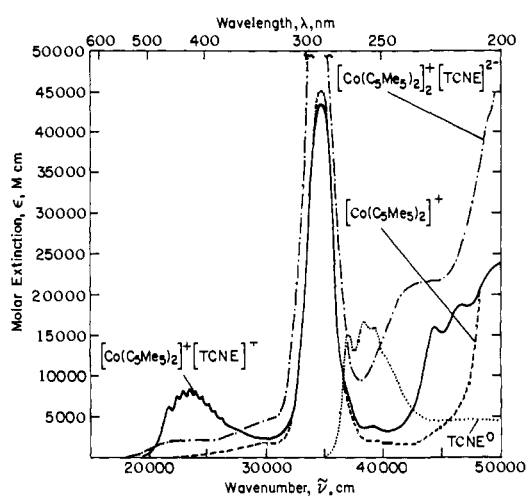


Figure 6. Electronic absorption spectra of TCNE, $[\text{Co}(\text{C}_5\text{Me}_5)_2]^+[\text{TCNE}]^{2-}$, $[\text{Co}(\text{C}_5\text{Me}_5)_2]^+[\text{TCNE}]^-$, $\{[\text{Co}(\text{C}_5\text{Me}_5)_2]^+\}_2[\text{TCNE}]^{2-}$, and $[\text{Co}(\text{C}_5\text{Me}_5)_2]^+[\text{PF}_6]^-$.

and 2228^{21a} or $2263^{21b,c}$ (b_{3u}) cm^{-1} . The $\text{C}=\text{C}$ stretch is observed at 1569 (a_g) cm^{-1} . Our values are in good agreement with the previous studies.

For $[\text{TCNE}]^-$ we find a $\text{C}\equiv\text{N}$ stretching band in the Raman spectrum at 2185 cm^{-1} with both the $[\text{Fe}(\text{C}_5\text{Me}_5)_2]^{2+}$ and $[\text{Co}(\text{C}_5\text{Me}_5)_2]^+$ salts. The Raman for both the Fe and Co salts also has an intense band at 1412 cm^{-1} , assigned to the $\text{C}=\text{C}$ stretch. The infrared spectra show two $\text{C}\equiv\text{N}$ stretching bands at 2144 and 2183 cm^{-1} . The Raman spectra of the Na^+ and $\text{K}^+[\text{TCNE}]^-$ salts have been previously measured,^{21b,c} and a $\text{C}\equiv\text{N}$ stretching band at 2200 cm^{-1} (a_g) and a $\text{C}=\text{C}$ stretching band at 1392 cm^{-1} (a_{1g}) were reported. The difference in the $\text{C}\equiv\text{N}$ and $\text{C}=\text{C}$ stretching frequencies between our large, diffuse cation salts and the previously reported K^+ and Li^+ is probably due to a close electrostatic interaction between the alkali cation and the anion.

For $[\text{TCNE}]^{2-}$ we observe two infrared-active bands at 2069 and 2140 cm^{-1} . The assignment of these infrared bands will be given below. In the Raman spectrum for $[\text{TCNQ}]^{2-}$ we observe a $\text{C}\equiv\text{N}$ stretch at 2190 cm^{-1} and a $\text{C}-\text{C}$ stretch at 1340 cm^{-1} .

The variation of the symmetric $\text{C}\equiv\text{N}$ and the $\text{C}=\text{C}$ stretching frequencies with increasing negative charge is shown in Figure 5. The $\text{C}=\text{C}$ stretches decrease as negative charge is added. This is consistent with the change in the formal bond order of 2 ($n = 0$) to 1 ($n = 2^-$). For the $\text{C}\equiv\text{N}$ stretch, the frequency drops from $n = 0$ to $n = 1^-$ and shows a slight increase of 4 cm^{-1} from $n = 1^-$ to $n = 2^-$. This leveling effect is probably due to the change in molecular structure from D_{2h} for $n = 1^-$ to D_{2d} symmetry for $n = 2^-$.

Table IV. Summary of Electronic Spectra for $[\text{TCNE}]^n$ ($n = 0, 1^-, 2^-$)^a

	λ_{max} , nm	λ_{max} , cm^{-1}	ϵ , $\text{M}^{-1} \text{cm}^{-1}$
TCNE	270	37 000	15 000
	261	38 300	16 750
	255	39 200	15 880
	248 sh	40 300	11 800
	219	45 700	4 540
$[\text{TCNE}]^{2-}$	230	44 450	21 545
$[\text{TCNE}]^{1-}$	471	21 230	4 815
	461	21 705	6 285
	448	22 300	7 440
	438	22 820	8 205
	428	23 375	8 425
	419	23 890	8 020
	410	24 445	7 305
	400	25 000	6 435
	392	25 515	4 775
	376	26 625	4 100
	368	27 185	3 585
	361	27 740	3 100
	354	28 255	2 950
	346	28 890	2 775
	339	29 525	2 600
	333	30 000	2 300
	225	44 435	15 900
	215	46 500	18 600

^a MeCN.

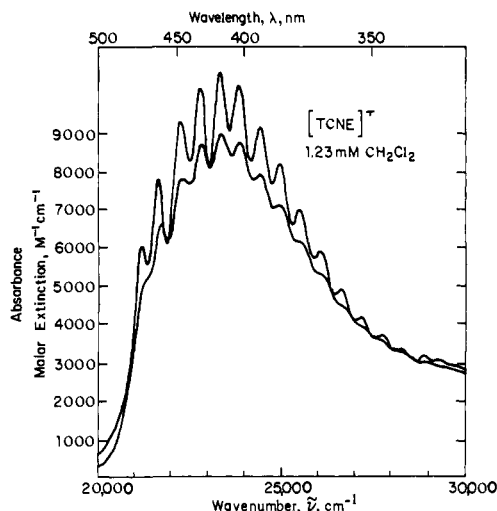


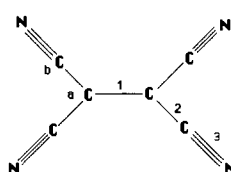
Figure 7. UV-vis spectra of $[\text{TCNE}]^{1-}$. Showing 17 vibrational overtones.

Electronic Spectra. The UV-visible spectra for TCNE, $[\text{Co}(\text{C}_5\text{Me}_5)_2]^+[\text{TCNE}]^-$, and $\{[\text{Co}(\text{C}_5\text{Me}_5)_2]^+\}_2[\text{TCNE}]^{2-}$ are shown in Figure 6 and summarized in Table IV together with the spectrum for $[\text{Co}(\text{C}_5\text{Me}_5)_2]^+[\text{PF}_6]^-$. The TCNE spectrum is characterized by a single absorption with some fine structure. The peak at $38\,300$ cm^{-1} is assigned to the $\Pi \rightarrow \Pi^*$ transition, and the structure could be assigned to coupling of a vibrational transition of ~ 1200 cm^{-1} . Since the transition is allowed, the vibrational progression is probably the $\text{C}=\text{C}$ stretch which is at lower energy in the excited state due to a decrease in the bond order of the $\text{C}=\text{C}$ bond as compared to the ground state.

The electronic absorption spectrum for $[\text{TCNE}]^{1-}$ is characterized by a number of sharp spectral features (Figure 6).²² An absorption with fine structure has an onset at $20\,000$ cm^{-1} . The intense absorption near $35\,000$ cm^{-1} is due to the cation. A partially structured absorption beginning near $42\,000$ cm^{-1} can be attributed to the anion although near $50\,000$ cm^{-1} , the cation begins absorbing again.

The most interesting portion of the spectrum for $[\text{TCNE}]^{1-}$ is the structured visible transition at $23\,375$ cm^{-1} (Figure 7; Table

(22) This has previously been noted by: Webster, O. W.; Mahler, W.; Benson, R. E. *J. Am. Chem. Soc.* **1962**, *84*, 3678.

Table V. Calculated and Average Observed Geometric Parameters for $[TCNE]^n$ ($n = 0, 1-, 2-$)^a


	$r(\text{C}-\text{C})$ 1	$r(\text{C}-\text{CN})$ 2	$r(\text{C}\equiv\text{N})$ 3	$\theta(\text{NC}-\text{C}-\text{CN})$ a	$\theta(\text{C}-\text{C}\equiv\text{N})$ b	energy (SCF)	energy (MP-2)
$n = 0$ (STO-3G)	1.344	1.460	1.158	116.6	179.8	-439.252 070	-439.970 852
$n = 0$ (DZ + D _c)	1.340	1.439	1.150	116.5	179.6	-444.783 156	-445.829 846
$n = 0$ (expt) ¹⁸	1.355	1.431	1.160	116.1	177.9		
$n = 1-$ (STO-3G)	1.430	1.427	1.179	118.4	178.7	-439.238 858	
$n = 1-$ (expt) ^{3b}	1.392	1.417	1.140	117.7	179.9		
$n = 1-$ (expt) ²⁵	1.370	1.444	1.138	c	c		
$n = 2-$ (STO-3G)	1.494	1.413	1.167	115.0	179.4	-438.953 273	-439.609 808
$n = 2-$ (DZ + D _c)	1.491	1.409	1.176	115.0	179.4	-444.784 395	-445.833 463
$n = 2-$ (DZ + D _c + Dif)	1.486	1.407	1.175	115.2	179.4	-444.788 699	-445.842 560
$n = 2-$ (DZ + D _c + All)	1.491	1.407	1.173	115.1	179.4	-444.804 771	
$n = 2-$ (STO-3G)pl ^d	1.535	1.398	1.170	116.5	178.5	-438.937 368	-439.596 199
$n = 2-$ (DZ + D _c)pl	1.517	1.398	1.178	115.7	179.1	-444.768 213	-445.818 076
$n = 2-$ (DZ + D _c + Dif)pl	1.514	1.396	1.177	115.6	179.1	-444.773 028	-445.828 337
$n = 2-$ (DZ + D _c + All)pl	1.515	1.396	1.175	115.5	179.3	-444.789 431	
$n = 2-$ (expt) ^b	1.49	1.393	1.166	117.0	177.6		

^a Bond distances in Å; bond angles in deg; energies in au. ^b This work. ^c No reported. ^d pl = planar.

IV). Following previous work^{23,24} we assign this transition as an internal transition. The orbital occupancy for $[TCNE]^n$ (in terms of the TCNE orbitals) is $(\Pi)^2(\Pi^*)^1$ whereas the lowest excited state should be $(\Pi)^1(\Pi^*)^2$. Since this transition only involves occupied orbitals of the monoanion, we define it as an internal transition. The symmetry of the ground state is ${}^2B_{2u}$ while that of the excited state is ${}^2B_{3g}$; this produces an allowed transition which is z-polarized (B_{1u}). Since the transition is allowed, the observed vibrations should be totally symmetric and representative of the excited-state vibrations. The spacing of the bands (~ 550 cm^{-1}) is consistent with a vibrational transition. In TCNE there is an a_g vibrational transition at 541 cm^{-1} assigned to the C—C≡N bend. In the anion the observed a_g transition at 532 cm^{-1} can also be assigned to this mode (vide infra). We thus expect that this transition is the one observed in the excited state. Such a bending transition (at 331 cm^{-1}) is also observed for the internal transition in $[TCNQ]^{\cdot-}$.²⁴ The C=C stretches are not observed in this transition although such a stretch is observed in the transition for $[TCNQ]^{\cdot-}$.²⁴ We do note that there is significant cyano character in the Π^* orbital of TCNE (vide infra).

The higher energy transition is probably from the SOMO to the unoccupied orbitals and is consistent with other studies.²³ There are two unoccupied TCNE orbitals above the Π^* with significant C≡N character. These orbitals are split by 2100 cm^{-1} with the lower orbital of a_g symmetry and the upper orbital of b_{1u} symmetry. Transitions from the ground state to the upper orbital are allowed and are y-polarized (b_{2u}). The peak separations are approximately 2200 cm^{-1} , consistent with excitation of the C≡N stretches.

The spectrum for $[TCNE]^{2-}$ shows no structure attributable to the dianion except for the onset of the peak near $40\,000$ cm^{-1} which is red-shifted from that in $[TCNE]^{\cdot-}$. Since the geometry for $[TCNE]^{2-}$ is significantly different from that in $[TCNE]$ and $[TCNE]^{\cdot-}$ the transitions may be localized on the $[C(CN)_2]^-$ groups.

Theoretical Results

Structures. The calculated geometric parameters are given in Table V and are compared to the average experimental values. The calculated $n = 0$ and $n = 1-$ structures have planar D_{2h} structures as confirmed by our force field calculations while the

$n = 2-$ structure has D_{2d} symmetry again confirmed by our force field calculations.

The geometric trends with the STO-3G basis differ somewhat from the observed trends although we do note that we are comparing RHF and UHF calculations so our comparison is not rigorous. The value for $r(\text{C}=\text{C})$ does increase with increasing negative charge just as observed experimentally. However, the theory predicts that the C—CN bond distance should continuously decrease with increasing negative charge. This may be a theoretical artifact as there is a 0.03 -Å difference between the experimental and calculated values for $r(\text{C}-\text{CN})$ for TCNE. However, it does suggest that it may be useful to reinvestigate the structure of $[TCNE]^{\cdot-}$ by using neutron diffraction techniques. The calculated trend in $r(\text{C}\equiv\text{N})$ is that it increases from $n = 0$ to $n = 1-$ but then decreases for $n = 2-$. This is again opposite to the experimental trend but is probably due to a deficiency in the UHF method (vide infra). The unusual experimental trend in $\theta(\text{NC}-\text{C}-\text{CN})$ of an increase and then a decrease in going from $n = 0$ to $n = 1-$ to $n = 2-$ is reproduced by theory. We do note that the calculated and experimental trends for $n = 0$ and $n = 2-$ are well-reproduced by the theory.

Although the DZ + D_c basis set can be employed for $[C-(CN)_3]^{-5}$ and $[C_2(CN)_4]^n$ ($n = 0, 2-$), due to the large number of basis functions it is almost impractical to use it for larger cyano-substituted systems (e.g., there are 102 basis functions for $[C_2(CN)_4]^n$). Thus, we have compared the STO-3G basis to the results from the better basis set to demonstrate the quality of the STO-3G results. The STO-3G parameters are in excellent agreement with the parameters from the larger basis set with the largest discrepancy being the difference in $r(\text{C}-\text{CN})$ for $n = 0$ of 0.021 Å. Thus, the larger basis set is in better agreement with experiment although the theoretical distance for $r(\text{C}\equiv\text{N})$ is, surprisingly, slightly longer. The STO-3G basis set does provide an adequate description of the molecular geometries. Inclusion of the diffuse functions on the ethylenic carbons and on all atoms does not lead to any changes in the geometry of the dianion as compared to that obtained with the DZ + D_c basis set.

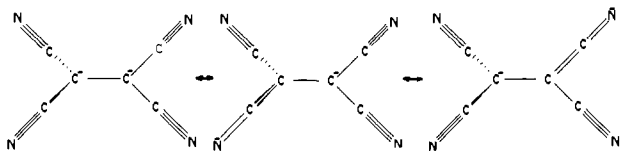
It is of interest to compare $r(\text{C}-\text{CN})$ and $r(\text{C}\equiv\text{N})$ for $n = 2-$ with those parameters from $[C(CN)_3]^-$ at the DZ + D_c level.⁵ The respective bond distances for $[C(CN)_3]^-$ are 1.413 and 1.165 Å which are similar to the values of 1.409 and 1.176 Å found for $[TCNE]^{2-}$. The C≡N bond distance in $[TCNE]^{2-}$ is somewhat longer than the distance in $[C(CN)_3]^-$. This is consistent with there being only two centers to which charge can be delocalized in $[C_2(CN)_4]^{2-}$ as opposed to three centers in $[C(CN)_3]^-$; thus, each alternate resonance structure in $[C_2(CN)_4]^{2-}$ must play a

(23) Miller, J. S.; Krusic, P. J.; Dixon, D. A.; Reiff, W. M.; Zhang, J. H.; Epstein, A. J. *J. Am. Chem. Soc.* **1986**, *108*, 4459.

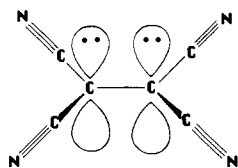
(24) Haller, I.; Kaufman, F. B. *J. Am. Chem. Soc.* **1976**, *98*, 1464.

(25) Flandrois, S.; Ludolf, K.; Keller, H. J.; Nothe, D.; Bondeson, S. R.; Soos, Z. G.; Wehe, D. *Mol. Cryst. Liq. Cryst.* **1983**, *95*, 149.

larger role. The shorter C—CN bond in [TCNQ]²⁻ is also consistent with this result.



We also examined a D_{2h} form of the dianion with all of the basis sets. It is a transition state characterized by a simple imaginary frequency and is 9.8 kcal/mol higher in energy at the SCF level, 8.9 at the MP-2 level,²⁶ with the DZ + D_C + Dif basis set. The rotational barrier shows little variation with basis set and the remaining values are as follows: 10.0 (SCF), 8.5 (MP-2) with the STO-3G basis set; 10.1 (SCF), 9.7 (MP-2) with the DZ + D_C basis set; and 9.6 (SCF) with the DZ + D_C + All basis set. As expected the C—C bond lengthens to 1.515 Å (DZ + D_C + All basis set) due to repulsion of the two electrons present in the Π^* orbital. Alternatively, in valence bond terms, this can be considered as the repulsion of two lone pairs in the [C(CN)₂]⁻ groups that are separated by a single bond:



The C≡N bonds lengthen slightly while the C—CN bond shortens by ~0.01 Å in the planar form. This is consistent with a small delocalization of negative charge onto the cyano groups, thereby lowering the repulsion between the two carbanion centers. The bond angle $\theta(\text{NC—C—CN})$ is predicted to open up slightly in the planar form.

Vibrational Spectra. The calculated frequencies with both basis sets are given in Table VI together with their infrared intensities for planar D_{2h} [TCNE]ⁿ ($n = 0, 1-, 2-$). We have also included scaled frequencies in order to account for our neglect of correlation effects and anharmonic corrections. For the STO-3G basis set, we employ a scaling factor of 0.82 for $\nu > 1800 \text{ cm}^{-1}$ and a scaling factor of 0.90 for the remaining frequencies. For the frequencies calculated with the DZ + D_C and DZ + D_C + Dif basis sets, the cyano frequencies were scaled by 0.88 and the remaining frequencies were scaled by 0.90.

There is reasonably good agreement between the two sets of scaled frequencies for TCNE. Differences are found for the CC stretch where the DZ + D_C value is higher by 52 cm^{-1} , suggesting a smaller scale factor. The second highest b_{2g} mode at the STO-3G level is 38 cm^{-1} higher than the DZ + D_C value, and the STO-3G value for the second highest b_{3u} frequency is high by 29 cm^{-1} . All of the others agree within 20 cm^{-1} except for the highest b_{3g} frequency which is 22 cm^{-1} higher with the STO-3G basis set.

The two sets of experimental frequencies for TCNE show only a few differences.^{21a,b} Good agreement of the scaled cyano frequencies with the experimental values is found. We do not calculate as large a splitting in the cyano frequencies as is observed experimentally, and we predict the two infrared active transitions to be very close in energy. Our scaled DZ + D_C frequency for the C=C stretch is high, and a scaling factor of 0.86 seems more appropriate. In terms of the third highest a_g mode we prefer neither assignment and suggest that the band is nearer to 600 cm^{-1} . The b_{1g} transition at 416 cm^{-1} given as questionable in ref 21a is probably a correct assignment as is the assignment of a band at 510 cm^{-1} (b_{2g}). However, the assignment of the transitions for

the b_{2u} modes by ref 21a is incorrect. The higher transition is probably ~600 cm^{-1} or slightly higher while the 442 cm^{-1} transition is far too high and should be closer to 160 cm^{-1} . Similarly the b_{3g} transitions are not correctly assigned. There should be a transition near 740–750 cm^{-1} and one near 275 cm^{-1} , not the 596 and 360 cm^{-1} ones reported in ref 21a.

The DZ + D_C intensities are probably more accurate than the STO-3G intensities since the former is a better basis set. In general the qualitative agreement for TCNE (weak, medium, strong) is good. The major differences are that the STO-3G basis set gives much larger cyano stretching intensities, and the b_{1u} mode near 960 cm^{-1} is predicted to be quite intense by the DZ + D_C basis set and very weak at the STO-3G level.

The UHF calculations on [TCNE]⁻ do not give imaginary frequencies; thus, the D_{2h} structure is a minimum on the potential energy surface. As discussed above, the C≡N bond lengths are too long at this level of calculation. Consequently the frequencies are too low, and we cannot examine how the cyano frequencies vary as a negative charge is added. The C=C frequency is properly treated since a scale factor of 0.85 is needed to get agreement with experiment. The remaining frequencies do not show any dramatic changes except that the out-of-plane modes significantly decrease in energy as expected since the compound does have an electron in a Π^* orbital.

Comparison of the calculated spectrum for [TCNE]⁻ with experiment^{21b,c} shows that the a_g band at 464 cm^{-1} may be misassigned or is showing a large interaction with the alkali counterion. We suggest that there should be a band at about 615 cm^{-1} and that the band at 464 cm^{-1} is misidentified and actually may be a b_{3u} band which is calculated at 456 cm^{-1} .

The infrared spectrum of the dianion has fewer observable transitions due to the D_{2d} symmetry. The calculated and scaled values are given in Table VII. The scaling factors are those used for TCNE. Comparison of the STO-3G and DZ + D_C basis sets for the dianion again shows reasonable agreement for the scaled frequencies although the differences seem somewhat larger than what was found for TCNE. This may be due to the need for different scale factors. The agreement between the frequencies and the intensities determined with the DZ + D_C and DZ + D_C + Dif basis sets is excellent. Thus, as found above for the geometric parameters, the diffuse functions do not play an important role in defining the shape of the potential energy hypersurface near the minimum if a good quality basis set is used as a starting point.²⁷ Both basis sets predict a large difference between the degenerate e cyano stretching modes and the nondegenerate a and b_2 stretching modes. Comparison with the neutral C≡N modes shows shifts of 100–200 cm^{-1} . The "C=C" mode is also expected to show a significant shift of almost 300 cm^{-1} .

The infrared intensities from the calculations are again in qualitative agreement. All predict that the C≡N stretching modes should be quite intense; in this case, the larger basis sets give the larger intensities. The three basis sets also predict a significant enhancement of the intensities of the C≡N stretches in the presence of the two negative charges. This has been predicted for [TCNQ]^{2-20a} and is due to the more polarizable charge distribution in the dianion leading to a larger $d\mu/dq$ term where μ is the dipole moment and q is the normal coordinate. With the DZ + D_C basis set, the C≡N stretching frequencies are more intense in [TCNE]²⁻ than in TCNE.

There are three vibrational transitions associated with the cyano stretches. The e and b_2 modes are the infrared-active modes. We calculate the e mode to be lower in frequency. We thus assign the experimental infrared cyano modes as 2069 (e) and 2140 cm^{-1} (b_2). These assignments suggest that the scaling factors for the cyano stretches in [TCNE]²⁻ should be 0.92 for the b_2 mode and 0.93 for the e mode rather than 0.88 taken for TCNE.

The variation of the observed and calculated symmetric C≡N and the C=C stretching frequencies with charge are shown in Figure 5. The general variations are the same with the cyano frequency, however, varying less than the C=C stretching frequency. The calculated cyano frequencies show a larger variation with charge than found experimentally. Both the STO-3G and

(26) (a) Moller, C.; Plesset, M. S. *Phys. Rev.* **1934**, *46*, 618. (b) Pople, J. A.; Binkley, J. S.; Seeger, R. *Int. J. Quantum Chem. Symp.* **1976**, *10*, 1.

(27) A similar result is observed by: Hehre, W. J.; Radom, L.; Schleyer, P. v. R.; Pople, J. A. *Ab initio Molecular Orbital Theory*; Wiley: New York, 1986; pp 204–212.

Table VI. Vibrational Frequencies for Planar D_{2h} [TCNE] n ($n = 0, 1-, 2-$)

symmetry ^b label	$n = 0$						$n = 1-$				
	ν (STO-3G)	ν_{scale}^- (STO-3G) ^c	I (STO-3G)	ν (DZ + D _c)	ν_{scale}^- (DZ + D _c)	I (DZ + D _c)	ref 21a	ref 21b	ν (STO-3G)	ν_{scale}^- (STO-3G) ^c	ref 21b
a _g	2717	2228	0.0	2537	2233	0.0	2236	2235	2108	(2108) ^d	2200
	1932	1584	0.0	1818	1636	0.0	1569	1569	1658	1409	1392
	676	608	0.0	667	600	0.0	679	535	683	615	532
	601	541	0.0	588	529	0.0	541	490	605	544	464
a _u	133	120	0.0	143	129	0.0	127	130	177	159	
	552	497	0.0	547	492	0.0			475	428	
b _{1g}	90	81	0.0	90	81	0.0			65	58	
	445	400	0.0	458	412	0.0	416 (?)		467	420	
b _{1u}	2730	2237	66	2550	2244	5.1	2260	2230	1941	(1941) ^d	
	1074	967	1.3	1055	950	2.9	958	958	967	870	970
	669	602	2.1	658	592	1.2	578	579	647	582	
	171	154	11	178	160	12	165	165	145	130	
b _{2g}	2719	2230	0.0	2545	2240	0.0	2247	2247	1958	(1958) ^d	
	1452	1307	0.0	1410	1269	0.0	1280	1282	1366	1229	
	593	534	0.0	582	524	0.0	510		579	521	
	301	271	0.0	307	276	0.0	253	254	277	249	
b _{2u}	693	624	1.9	682	614	0.8	554 (?)		551	496	
	171	154	24	175	158	29	442 (?)		162	146	
b _{3g}	846	761	0.0	821	739	0.0	596 (?)		587	528	
	299	269	0.0	310	279	0.0	360 (?)		290	261	
b _{3u}	2723	2233	138	2548	2242	3.8	2228	2263	1965	(1965) ^d	
	1280	1152	41	1248	1123	74	1155	1155	1233	1110	1187
	524	468	0.1	523	471	0.3	426	443	507	456	
	112	101	3.4	124	112	4.2	119		122	110	

symmetry ^b label	$n = 2-$								
	ν (STO-3G)	ν_{scale}^- (STO-3G) ^c	I (STO-3G)	ν (DZ + D _c)	ν_{scale}^- (DZ + D _c)	I (DZ + D _c)	ν (DZ + D _c + Dif)	ν_{scale}^- (DZ + D _c + Dif)	I (DZ + D _c + Dif)
a _g	2628	2155	0.0	2355	2072	0.0	2358	2075	0.0
	1538	1307	0.0	1427	1284	0.0	1432	1289	0.0
	764	688	0.0	717	645	0.0	719	647	0.0
	565	508	0.0	534	481	0.0	540	486	0.0
a _u	147	132	0.0	153	138	0.0	153	138	0.0
	529	476	0.0	551	496	0.0	545	490	0.0
	56i	50i	0.0	57i	51i	0.0	58i	52i	0.0
b _{1g}	586	527	0.0	597	537	0.0	592	533	0.0
	b _{1u}	2597	2130	201	2309	2032	533	2311	2033
1149		1034	2.3	1094	985	42	1099	989	40
749		674	0.7	703	633	4.4	704	634	6.3
188		169	18	191	172	26	191	172	26
b _{2g}	2472	2027	0.0	2165	1905	0.0	2168	1908	0.0
	1375	1238	0.0	1364	1228	0.0	1366	1229	0.0
	633	570	0.0	613	552	0.0	614	553	0.0
	299	269	0.0	294	265	0.0	294	265	0.0
b _{2u}	597	537	136	629	566	55	621	559	42
	135	122	4.6	134	121	11	140	126	12
b _{3g}	562	506	0.0	615	554	0.0	624	562	0.0
	247	222	0.0	218	196	0.0	258	232	0.0
b _{3u}	2483	2036	1273	2199	1935	2789	2201	1937	2845
	1300	1170	321	1271	1144	149	1275	1148	166
	567	510	9.2	559	503	8	559	503	8
	113	102	0.1	122	110	0.1	122	110	0.1

^a Frequencies in cm^{-1} . Intensities in km/mol . ^b Symmetry labels for a D_{2h} structure. The C=C axis is the z axis, and xz is the molecular plane. The labeling follows the convention in; Cotton, F. A. *Chemical Applications of Group Theory*, 2nd ed.; Wiley-Interscience: New York, 1971. ^c Scaled frequencies. See text. ^d Unscaled. See text. ^e Scaled by 0.85. Scale factor for $\nu[\text{C}=\text{C}]$ from $n = 1-$.

the experimental C=C stretches show the leveling effect discussed above with a larger difference found going from $n = 0$ to $n = 1-$ than from $n = 1-$ to $n = 2-$.

We also calculated the vibrational spectrum for the D_{2h} planar structure for the dianion with the three basis sets (Table VI). This structure is a transition state characterized by one imaginary frequency (a_u torsion) at $58i \text{ cm}^{-1}$ (DZ + D_c + Dif). Comparison with the optimum D_{2d} structure for the dianion shows that the cyano stretching frequencies are still split by almost 200 cm^{-1} . This is similar to what is found in [TCNQ] $^{2-}$ where a large splitting of the CN frequencies in the dianion is also observed.^{20c,28} The C-C stretching frequency is significantly lower in D_{2h} [TCNE] $^{2-}$ than in TCNE and is about 20 cm^{-1} higher than that in the D_{2d} structure for [TCNE] $^{2-}$. Most of the other frequencies

do not show significant changes on rotation about the C-C bond in [TCNE] $^{2-}$. The only difference in the results for the DZ + D_c and DZ + D_c + Dif basis sets is in the second out-of-plane b_{3g} mode where the larger basis set gives a higher frequency by 40 cm^{-1} .

One of the more interesting changes is the increase in the C-CN stretching frequencies in the planar dianion as compared to those in TCNE. Only the b_{2g} stretch decreases in the dianion; the other three stretches increase. The a_g and b_{1u} stretches increase by almost 40 cm^{-1} each. Also of interest is the 200 cm^{-1} decrease in the highest b_{3g} mode in the dianion and the 60 cm^{-1} decrease for the highest b_{2u} mode. The third b_{1u} mode increases by $\sim 50 \text{ cm}^{-1}$ in the dianion, and the third b_{3u} mode increases by $\sim 40 \text{ cm}^{-1}$.

Charge and Spin Distributions. The Mulliken charge and spin populations with the STO-3G basis set are given in Table VIII. As expected the negative charge on nitrogen increases as negative

Table VII. Infrared Vibrational Frequencies and Intensities for D_{2d} [TCNE] $^{2-}$ ^a

symmetry label	ν (STO-3G)	ν_{scale}^* (STO-3G)	I (STO-3G)	ν (DZ + D _c)	ν_{scale}^* (DZ + D _c)	I (DZ + D _c)	ν (DZ + D _c + Dif)	ν_{scale}^* (D _c + Dif)	I (DZ + D _c + Dif)
a ₁	2605	2136	0.0	2334	2054	0.0	2338	2057	0.0
	1441	1297	0.0	1402	1262	0.0	1413	1272	0.0
	763	687	0.0	720	648	0.0	719	647	0.0
	580	522	0.0	548	493	0.0	552	497	0.0
	136	122	0.0	142	128	0.0	140	126	0.0
a ₂	629	566	0.0	627	564	0.0	623	561	0.0
b ₁	570	513	0.0	586	527	0.0	580	522	0.0
	49	44	0.0	48	43	0.0	43	39	0.0
b ₂	2624	2152	143	2333	2053	482	2338	2057	508
	1138	1024	3.2	1073	966	30	1076	968	27
	751	676	0.0	713	642	1.0	712	641	1.2
	185	166	15.	194	175	22	191	172	22
e	2512	2060	492	2223	1956	1208	2226	1959	1230
	1252	1127	100	1252	1127	38	1256	1130	45
	667	600	39	661	595	41	657	591	33
	582	524	44	583	525	9	578	520	9
	320	288	0.1	319	287	0.3	318	286	0.1
	103	93	1.2	93	84	2.8	93	84	3.0

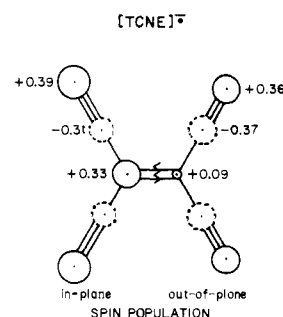
^a frequencies in cm⁻¹; intensities in km/mol.**Table VIII.** Charge and Spin Distributions in [TCNE] $^{n-}$ ($n = 0, 1-, 2-$)^a

Mulliken Charge Populations (STO-3G Basis)					
atom	$n = 0$	$n = 1-$	$n = 2-$ (D_{2d})	$n = 2-$ (D_{2h})	
C(CN) ₂ (sp ²)	0.07	-0.07	-0.19	-0.19	
CN (sp)	0.09	0.05	0.03	0.02	
N	-0.12	-0.26	-0.43	-0.43	
Mulliken Charge Populations (Larger Basis Sets)					
atom	$n = 0$	$n = 2-$ (D_{2d})		$n = 2-$ (D_{2h})	
		DZ + D _c	DZ + D _c + Dif	DZ + D _c	DZ + D _c + Dif
C(CN) ₂ (sp ²)	0.16	-0.23	-0.25	-0.20	-0.19
CN (sp)	-0.09	-0.06	-0.04	-0.07	-0.07
N	0.02	-0.32	-0.34	-0.32	-0.33
Spin Population in [TCNE] $^{n-}$					
	total	p _z	p _x , p _y	s	spin density
C(CN) ₂ (sp ²)	0.49	0.33	0.09	0.06	0.16
CN (sp)	-0.77	-0.31	-0.37	-0.11	-0.28
N	0.79	0.39	0.36	0.04	0.12

^a Populations in electrons.

charge is added to TCNE. The ethylenic sp² carbons also become increasingly negative while the CN sp carbon charge varies slightly. The charge distribution for the D_{2h} structure of [TCNE] $^{2-}$ is the same as those for the D_{2d} structure. The trends in the DZ + D_c charges for $n = 0$ and $n = 2-$ follow the STO-3G values for TCNE. For [TCNE] $^{2-}$ there is less negative charge on the nitrogens with the larger basis set, reflecting the values found in TCNE. Again there is essentially no difference between the DZ + D_c and DZ + D_c + Dif basis sets.

The UHF calculations on [TCNE] $^{n-}$ provide information about the spin density (Table VIII). There is one excess α -spin electron in [TCNE] $^{n-}$, and we define excess α -spin as positive and excess β -spin as negative. The total spin population shows a positive value on the sp² C and N (excess α -spin) and a negative value on sp C (excess β -spin). The excess spins on the sp C and N approximately cancel each other. The excess spin can be assigned to various orbital components. For the sp C and N the spin is about evenly divided between the in-plane and out-of-plane 2p orbitals

**Figure 8.** Spin distribution for [TCNE] $^{2-}$.

(Figure 8). For the sp² C, most of the excess spin is in the out-of-plane 2p orbital, although there is a small in-plane 2p component. For the sp² C, the in-plane 2p component is comparable in size to the 2s component. The spin populations in the 2s orbitals are nonzero. The ESR hyperfine splitting is governed by the 2s spin populations since the only electron spin-nuclear spin interactions with a nonzero component are those involving s orbitals. On the basis of the 2s orbital populations and the spin densities, we would assign the largest ¹³C hyperfine splitting to be at the sp C and a smaller splitting of opposite sign at the sp² C.

Acknowledgment. We thank C. Vazquez for sample preparation, B. Chase and E. Mathews for the vibrational spectra and J. V. Caspar, R. Hilmer, and D. Wipf for the digitized electronic spectra.

Registry No. TCNE, 670-54-2; [TCNE] $^{n-}$, 77448-92-1; [TCNE] $^{2-}$, 56588-92-2; [Co(C₅Me₅)₂]₂[TCNE]·MeCN, 108120-01-0; [Co(C₅Me₅)₂]₂[TCNE], 108120-00-9; [Co(C₅Me₅)₂]⁺[TCNE] $^{n-}$, 108120-02-1; [Co(C₅Me₅)₂]⁺[PF₆] $^{-}$, 79973-42-5.

Supplementary Material Available: Tables of fractional coordinates and their estimated standard deviations, anisotropic thermal parameters, intramolecular bond angles, and weighted least-squares planes for {[Co(C₅Me₅)₂]⁺]₂[TCNE] $^{2-}$ ·MeCN (7 pages); a listing of calculated and observed structure factors for {[Co(C₅Me₅)₂]⁺]₂[TCNE] $^{2-}$ ·MeCN (19 pages). Ordering information is given on any current masthead page.